AGU PUBLICATIONS

JGR

Journal of Geophysical Research: Atmospheres

RESEARCH ARTICLE
10.1002/2015JD023858

Key Points:
- Significant intermodel spread in future projections of the eastern North Pacific subtropical high
- Cause for uncertain projections of winter precipitation changes in California
- Importance of atmosphere-ocean coupling in the North Pacific to reduce uncertainty

Supporting Information:
- Figures S1 and S2

Correspondence to:
S.-W. Son,
seokwooson@snu.ac.kr

Citation:
Choi, J., J. Lu, S.-W. Son, D. M. W. Frierson, and J.-H. Yoon (2016), Uncertainty in future projections of the North Pacific subtropical high and its implication for California winter precipitation change, *J. Geophys. Res. Atmos.*, *121*, 795–806, doi:10.1002/2015JD023858.

Received 26 JUN 2015
Accepted 2 JAN 2016
Accepted article online 7 JAN 2016
Published online 27 JAN 2016

Uncertainty in future projections of the North Pacific subtropical high and its implication for California winter precipitation change

Jung Choi[1], Jian Lu[2], Seok-Woo Son[1], Dargan M. W. Frierson[3], and Jin-Ho Yoon[2]

[1]School of Earth and Environmental Sciences (BK21), Seoul National University, Seoul, South Korea, [2]Pacific Northwest National Laboratory, Richland, Washington, USA, [3]Department of Atmospheric Sciences, University of Washington, Seattle, Washington, USA

Abstract This study examines future projections of sea level pressure change in the North Pacific and its impact on winter precipitation changes in California. The multimodel analysis, based on the Coupled Model Intercomparison Project phase 5 models under the Representative Concentration Pathway 8.5 scenario, shows a robust sea level pressure change in the late 21st century over the western North Pacific in which both the Aleutian Low and the North Pacific subtropical high (NPSH) shift poleward in concert with a widening of the Hadley cell. This change is partly explained by a systematic increase of static stability in the subtropics. Despite its robustness, the projected NPSH changes over the eastern North Pacific exhibit a substantial intermodel spread, contributing as a cause for uncertain projections of precipitation changes in California. This intermodel spread in the eastern North Pacific is associated with a Pacific Decadal Oscillation-like surface temperature change in the western North Pacific and the resulting meridional temperature gradient change. This study points to a major source of uncertainty for the response of winter precipitation to global warming over the West Coast of North America: atmosphere-ocean coupling in the North Pacific.

1. Introduction

Projected changes in regional and global precipitation in a warmer climate have been extensively documented in the literature. Based on both Coupled Model Intercomparison Project phases 3 and 5 (CMIP3 and CMIP5) model simulations, the Intergovernmental Panel on Climate Change recently reported that the hydrological contrast between wet and dry regions and between wet and dry seasons will likely increase in a warmer climate [*Intergovernmental Panel on Climate Change* (*IPCC*), 2013]. In terms of latitudinal distribution, this change, often referred to as the "rich-get-richer" mechanism, is characterized by more precipitation in the deep tropics and midlatitudes but less precipitation in the subtropics [e.g., *Held and Soden*, 2006]. These projected precipitation changes can be qualitatively described by the Clausius-Clapeyron relation, which relates the increase in water vapor with increasing air temperature [e.g., *Manabe and Wetherald*, 1975; *Held and Soden*, 2006]. However, precipitation changes are also known to be controlled by the large-scale atmospheric circulation such as the Hadley cell (HC) and extratropical storm tracks [e.g., *Lu et al*., 2007; *Scheff and Frierson*, 2012a].

The response of the atmospheric circulation to the increase in anthropogenic greenhouse gases is often characterized by a poleward expansion of the HC and poleward shift of the extratropical storm tracks [e.g., *Gerber and Son*, 2014; *Chang et al*., 2012]. These changes lead to a widening of the subtropical dry zone and a poleward shift of midlatitude rain belts [*Scheff and Frierson*, 2012a, 2012b; *Barnes and Polvani*, 2013; *Neelin et al*., 2013]. Among them, the projected dryness in the subtropics, which is associated with the HC expansion, has been primarily attributed to the increase of static stability in the subtropics with a nonnegligible contribution of the increased meridional temperature gradient near the tropopause level [e.g., *Lu et al*., 2008]. In a warmer climate, static stability is anticipated to increase as a result of the quasi-moist adiabatic temperature adjustment to the surface warming [e.g., *Frierson*, 2006]. This can stabilize the baroclinicity in the subtropics, resulting in a poleward displacement of the baroclinic instability and the related eddy-driven subsidence in the subtropics.

Many previous studies [e.g., *Frierson et al*., 2007; *Hwang et al*., 2013; *Seo et al*., 2014] have focused on the hydrological impacts of the changes in the zonal mean atmospheric circulation. However, regional precipitation changes, which vary significantly between regions, cannot be simply explained by the zonal mean atmospheric circulation changes [*IPCC*, 2013]. In general, regional climate projection is less robust than zonal mean or global mean climate

Table 1. Models Used in This Study[a]

No.	Model	Institution	No.	Model	Institution
1	ACCESS1-0	CSIRO-OM, Australia	19	GISS-E2-H	NASA, USA
2	ACCESS1-3		20	GISS-E2-H-CC	
3	bcc-csm1-1	BCC, China	21	GISS-E2-R	
4	bcc-csm1-1-m		22	GISS-E2-R-CC	
5	BNU-ESM	BNU, China	23	HadGEM2-CC	MOHC, UK
6	CanESM2	CCCma, Canada	24	HadGEM2-ES	
7	CCSM4	NCAR, USA	25	inmcm4	INM, Russia
8	CESM1-BGC		26	IPSL-CM5A-LR	IPSL, France
9	CESM1-CAM5		27	IPSL-CM5A-MR	
10	CMCC-CM	CMCC, Italy	28	IPSL-CM5B-LR	
11	CMCC-CMS		29	MIROC5	MIROC, Japan
12	CNRM-CM5	CNRM, France	30	MIROC-ESM	
13	CSIRO-Mk3-6-0	CSIRO-QCCCE, Australia	31	MIROC-ESM-CHEM	
14	FGOALS-g2	LASG, China	32	MPI-ESM-LR	MPI-M, Germany
15	FIO-ESM	FIO, China	33	MPI-ESM-MR	
16	GFDL-CM3	GFDL, USA	34	MRI-CGCM3	MRU, Japan
17	GFDL-ESM2G		35	NorESM1-M	NCC, Norway
18	GFDL-ESM2M		36	NorESM1-ME	

[a]The model acronyms were identified by the Fifth Assessment Report of the Intergovernmental Panel on Climate Change.

projection. This is particularly true for regions downstream of the jet where baroclinic eddies are prevalent. Recent studies have shown that future projections of atmospheric circulation changes downstream of the Pacific jet differ significantly among CMIP3 and CMIP5 models [*Chang*, 2013; *Neelin et al*., 2013; *Park and An*, 2014]. Such differences in the projected circulation changes are inevitably reflected in the projected changes in surface temperature and precipitation. For example, projected future precipitation changes in California show a substantial uncertainty [*Neelin et al*., 2013; *Chang et al*., 2015; *Langenbrunner et al*., 2015].

California usually receives half of its annual precipitation between December and February. As of the writing of this paper, California is entering the fourth year of one of its worst droughts in recorded history. To evaluate the degree to which greenhouse gas-induced global warming would affect California precipitation during the winter season and the related uncertainties, the present study examines the atmospheric circulation change over the North Pacific basin by using the state-of-the-art climate models. Specifically, future projections of the Aleutian Low (AL) and the North Pacific subtropical high (NPSH), which are the two dominant winter circulation systems affecting the hydroclimate in the North Pacific, and their impact on precipitation over California are analyzed. Only the boreal winter season (December–February; DJF), when both the AL and NPSH are well defined, is considered.

Unlike previous studies which are mainly based on upper tropospheric variables such as the westerly jet [*Neelin et al*., 2013; *Langenbrunner et al*., 2015], this study quantifies the lower tropospheric circulation using sea level pressure (SLP) field. SLP, whose variability and change represent mass redistribution in the atmosphere, is probably one of the most reliable variables among the reanalysis data sets [e.g., *Kalnay et al*., 1997] and has a long observational record. Although *Chang et al*. [2015] showed that SLP variance statistics (as a storm track activity) largely explain the intermodal spread in California precipitation projection, its physical mechanism(s) is still unclear. By examining the regional HC boundary and relevant scaling analysis, we provide a further insight on the projected large-scale circulation and California precipitation changes.

This paper is organized as follows. The data and methodology used in this study are described in section 2. The model performance in reproducing the climatological NPSH is first evaluated by comparing a multimodel ensemble (MME) with observations in section 3.1. The future projections are documented in section 3.2. In section 3.3, the intermodel spread in the projected NPSH changes and its uncertainty are discussed for the western and eastern North Pacific separately. A summary and discussion of this study are then presented in section 4.

2. Data and Methodology

As listed in Table 1, 36 CMIP5 models that have archived both the historical and Representative Concentration Pathway 8.5 (RCP8.5) simulations are used in this study. For a fair representation, only one ensemble member is

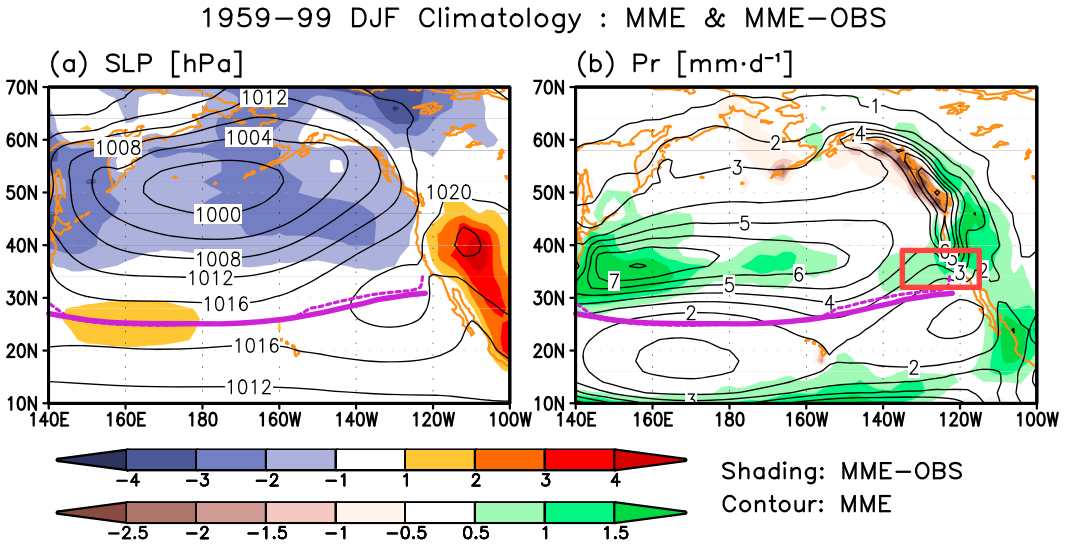

Figure 1. Contour lines indicate the multimodel ensemble (MME) climatology (1959–1999) for December-January-February (DJF) (a) sea level pressure and (b) precipitation from the CMIP5 historical simulation. Shading denotes the difference between the MME and observations. Here HadSLP2 (1959–1999) and GPCP (1979–1999) are used for the observations. Thick solid and dashed purple lines in Figures 1a and 1b indicate the locations of North Pacific subtropical high (NPSH) from MME and observation, respectively. The red box in Figure 1b includes the target area for California precipitation as reported by *Neelin et al.* [2013].

used for each model. All data sets are first interpolated onto a 2.0°×2.0° grid prior to analysis. The long-term climatology is then estimated as the average over the period of 1959–1999 from historical simulations. The projected future change is evaluated by computing the linear trend using a least squares fit over the period of 2007–2099 from RCP8.5 simulations. For reference, the model results are compared with the observed SLP from the Hadley Centre (HadSLP2) [*Allan and Ansell*, 2006] and the Japanese 55 years Reanalysis data (JRA-55) [*Kobayashi et al.*, 2015]. The Global Precipitation Climatology Project (GPCP) [*Adler et al.*, 2003] and the Climate Prediction Center Merged Analysis of Precipitation (CMAP) [*Xie and Arkin*, 1997] during period 1979–1999 are used for the evaluation of the model precipitation climatology.

It is often useful to define a climate index to concisely quantify an aspect of the atmospheric circulation. An example is the Northern Annular Mode index for the extratropical circulation in the Northern Hemisphere. In this study, regional circulation changes across the North Pacific are primarily quantified by changes in the latitudinal location of the NPSH, which is defined as the latitude where $dSLP/dy = 0$ [see also *Choi et al.*, 2014] (referred to as the NPSH latitude). As shown by *Hu et al.* [2011], the latitude of the zonal mean subtropical high dynamically coincides with the poleward edge of the HC, where the mass stream function changes sign. In addition, the surface zonal mean zonal wind changes sign at the latitude of the zonal mean subtropical high according to the vertically integrated geostrophic zonal mean momentum budget [*Choi et al.*, 2014].

To address the regional asymmetry of the NPSH and its long-term changes, two longitudinally averaged regions were considered across the dateline, which is the center of the AL, i.e., the western North Pacific (140°–180°E; hereafter, W-NPSH) and the eastern North Pacific (180°–120°W; hereafter, E-NPSH). The intermodel spread of the projected changes in W-NPSH and E-NPSH latitudes is then evaluated by analyzing the static stability and vertical wind shear changes over the North Pacific. To further characterize the relationship between the intermodel spread in the projected circulation changes over the eastern North Pacific and the uncertainty in the projected changes in California precipitation, a singular value decomposition (SVD) analysis is also performed.

3. Results

3.1. Climatology

Figure 1a shows the climatological DJF SLP in the historical simulations. The MME bias, which is the difference from observations (HadSLP2) over the time period of 1959–1999, is represented in shading. In general, except

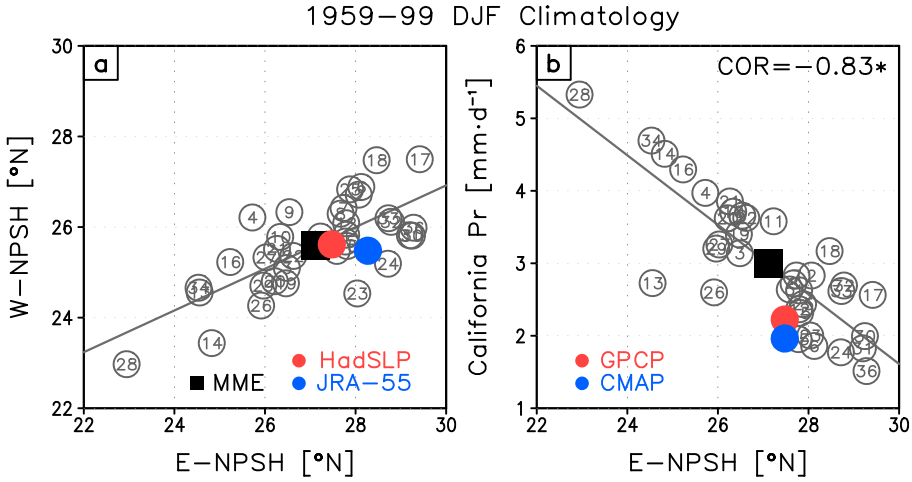

Figure 2. (a) Scatterplot of the climatological locations of the eastern NPSH (E-NPSH) and the western NPSH (W-NPSH). Each number denotes the model number as listed in Table 1. The filled square, red, and blue circles indicate the MME, HadSLP2, and JRA-55, respectively. (b) Same as Figure 2a but for E-NPSH latitudes and California precipitation (averaged over the red box area in Figure 1). Red and blue circles denote the precipitation from the GPCP and CMAP, respectively. Asterisks correspond to correlations that are statistically significant at the 95% confidence level.

over the continents, the SLP distribution is reasonably well reproduced by the MME, although the CMIP5 MME exhibits a slightly stronger NPSH and deeper AL than those in observations. When the SLP from JRA-55 is used as the reference, the MME bias becomes even smaller particularly around the center of the AL (see Figure S1a in the supporting information). Solid and dashed thick purple lines in Figure 1a denote the latitudinal locations of the NPSH as defined by the location of maximum SLP from the MME and observations, respectively. The NPSH is located between 25°N and 32°N in the observations except near the West Coast of North America. This longitudinal distribution is well reproduced by the MME, particularly for W-NPSH. Although the simulated E-NPSH is slightly biased equatorward, the difference between the MME and observations is not statistically significant.

The latitudinal locations of W-NPSH and E-NPSH in the individual models are further compared with observations in Figure 2a. In the HadSLP2 (JRA-55), denoted by the red (blue) dot, the W-NPSH and E-NPSH are located at approximately 25.6°N and 27.5°N (25.5°N and 28.3°N), respectively. As stated above, the MME reproduces these locations reasonably well, i.e., 25.6°N for W-NPSH and 27.1°N for E-NPSH. Although a weak equatorward bias is found in E-NPSH, the intermodel spread is substantially large, and the observed location of E-NPSH is within the uncertainty range of the model simulations.

The W-NPSH and E-NPSH latitudes are highly correlated with each other, with a correlation coefficient of 0.72, indicating a congruency between the upstream and downstream bias in the subtropical high (Figure 2a). However, the model-to-model spread of the E-NPSH latitudes is larger than that of W-NPSH latitudes. The standard deviations of the former and the latter are 1.52 and 0.97, respectively. In other words, the spread in model bias increases downstream of the Pacific jet where synoptic-scale eddy activity is more prevalent. This is somewhat expected due to the more vigorous eddy feedback to the mean flow downstream of the North Pacific storm track [e.g., *Chang et al.*, 2002].

Figure 1b presents MME precipitation and its departure from the GPCP observation during DJF. The observed climatology is computed for the period of 1979–1999, whereas the MME is computed for 1959–1999. Although not shown, the results are not sensitive to analysis period (e.g., MME for 1979–1999). In Figure 1b, two wet regions are identified in midlatitudes. The first is over the western North Pacific along the Kuroshio-Oyashio extension, and the second is along the upslope of Rockies. Across the Kuroshio-Oyashio extension, a large amount of heat and moisture are released, enhancing local precipitation and the Pacific storm tracks [e.g., *Kwon et al.*, 2010]. Although satellite estimation of precipitation is somewhat uncertain over the oceans (see Figure S1b), the MME generally overestimates the precipitation in the western North Pacific. Unlike the western North Pacific, the MME precipitation over the western United States and Canada is localized along

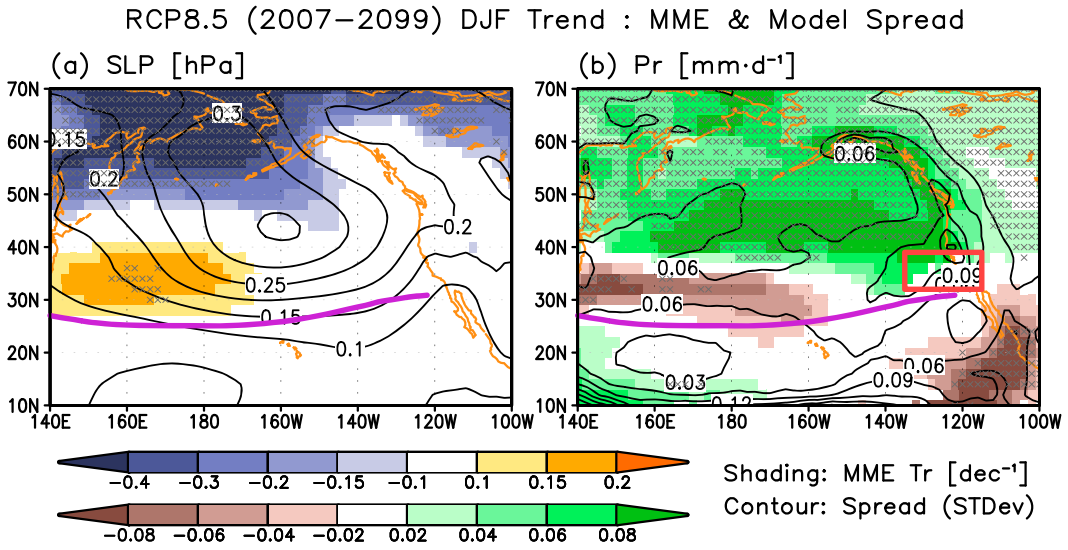

Figure 3. Future projections of DJF (a) sea level pressure and (b) precipitation changes over the period of 2007–2099 under the RCP8.5 scenario. The regions in which more than 66% of models (≥24) or 90% of models (≥32) have the same sign as the MME are represented by shading or hatches, respectively. Contours show the model spread (standard deviation) around the MME. The purple line in Figures 3a and 3b and the red box in Figure 3b are the same of those in Figure 1.

the Rockies and the Cascades, which is caused by uplifting by the windward slope of the topography on the incident storm track from the Pacific Ocean [*Chang*, 2013; *Neelin et al*., 2013]. The MME bias around these regions highly depends on the selected reference data but generally shows more diffused distribution of precipitation toward the downstream of the Rocky Mountains (see Figure S1b).

Focusing on the NPSH, we evaluate the relationship between California winter precipitation and the E-NPSH latitudes (Figure 2b). Here California precipitation is defined by averaging the precipitation in the red box in Figure 1b (135°–115°W, 32°–39°N), similar to *Neelin et al*. [2013]. The MME precipitation (about 3.00 mm/d) shows a wet bias in comparison to both GPCP (about 2.22 mm/d) and CMAP (about 1.96 mm/d) data. The intermodel spread indicates that California winter precipitation in the model is highly correlated with the latitudinal location of the E-NPSH with a correlation coefficient of −0.83 (Figure 2b). This result indicates that a negative bias in California precipitation in the model is related to a poleward bias of the E-NPSH latitude. Similar analyses are also performed for the intensity of the E-NPSH (i.e., maximum value of SLP over the eastern North Pacific) and the latitudinal location of the AL; their correlations with California winter precipitation are −0.68 and −0.52, respectively. This result suggests that the winter precipitation over California is more sensitive to the location of the subtropical high than that of the AL.

Neelin et al. [2013] showed that intermodel spread in the projected change of California winter precipitation is highly correlated with that of the Pacific jet extension index (i.e., areal averaged upper level zonal wind over California). For the climatology, their correlation is 0.71 (Figure S2a), slightly weaker than the correlation with E-NPSH latitude (Figure 2b). The latitudinal location of the E-NPSH is negatively correlated with the Pacific jet extension index at −0.57 (not shown). A negative correlation coefficient indicates that an equatorward shift of the E-NPSH is associated with a strengthening of the Pacific jet extension, and vice versa.

3.2. Future Projections

Future changes in winter SLP and precipitation under the RCP8.5 scenarios are shown in Figure 3. Regions where more than 66% and 90% of the models (≥24 and 32 models) have the same sign are shaded and hatched, respectively. Contours show the intermodel spread quantified by one standard deviation about the MME. Robust SLP trends are found only over 140°E–160°W with a dipolar structure about 45°N (shading in Figure 3a). On the poleward side of the western NPSH, shown by the thick purple line in Figure 3a, a relatively robust increase in SLP is also found. However, no robust change in SLP is found over the eastern North Pacific.

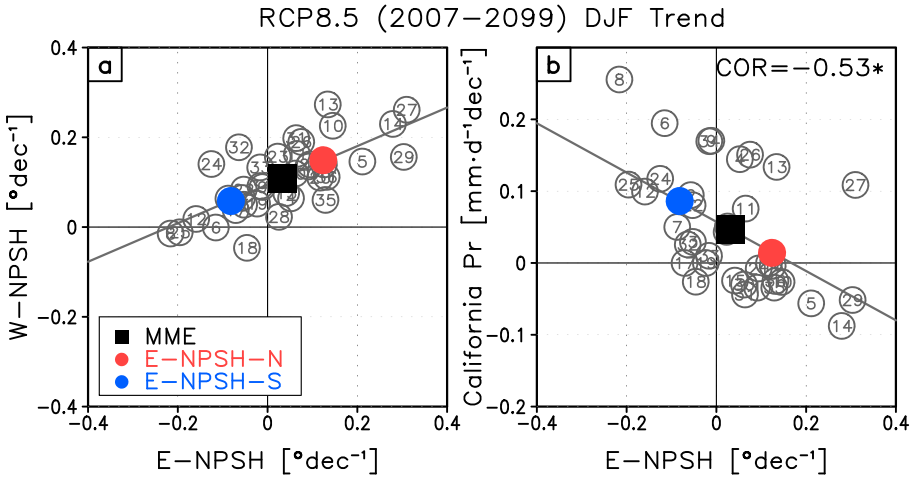

Figure 4. Same as Figure 2 but for the projected future changes of the E-NPSH and W-NPSH latitudes and California precipitation over the period of 2007–2099. The black square denotes the MME from all 36 models. Red and blue circles indicate the MME of the selected models showing positive and negative trends of E-NPSH latitudes, respectively.

Figure 4a shows the intermodel spread of the projected changes in the NPSH in terms of the linear trends of the W-NPSH and E-NPSH latitudes. Most models show a poleward shift in the W-NPSH (MME trend is 0.11°/decade). However, the projected shifts in the E-NPSH latitude are mixed among the models. Interestingly, the range of intermodel spread in E-NPSH latitude trends (−0.22 to 0.31) is much larger than that in W-NPSH latitude trends (−0.05 to 0.27). The red (blue) circles in Figure 4 further indicate the MMEs of 20 (16) models which show poleward (equatorward) shifts of E-NPSH latitude, at a rate of 0.12°/decade (−0.08°/decade). This large spread results in little MME change in the E-NPSH latitude (0.03°/decade). This result indicates that the uncertainty in the projected changes of NPSH latitudes increases downstream of the Pacific jet.

The projected changes in precipitation (Figure 3b, shading) show a significant increase in high latitudes but a decrease in low latitudes around the axis of maximum precipitation (Figure 1b). The dipole pattern of precipitation change is commonly explained by the thermodynamic response to global warming [*Held and Soden*, 2006; *Trenberth*, 2011]. However, there exists a large model-to-model spread, particularly near California region, as shown by the red box in Figure 3b. Previous studies [*Scheff and Frierson*, 2012b; *Neelin et al*., 2013; *Gao et al*., 2014; *Chang et al*., 2015; *Langenbrunner et al*., 2015] showed that future projection of California precipitation change is quite uncertain because of the geographical location of California and the large intermodel differences in the dynamical response to global warming such as displacements of the Pacific jet, subtropical dry zone, storm tracks, and expansion of the HC.

Figure 4b illustrates the relationship of the projected California precipitation change with the projected changes in the E-NPSH latitude. As in climatology (Figure 2b), they are linearly related with each other with a correlation coefficient of −0.53. A similar relationship, with an opposite sign, is also found, when the Pacific jet extension index [*Neelin et al*., 2013] is used, to explain the intermodel spread of California winter precipitation change (see Figure S2b, $r = 0.64$). Although the correlation coefficient shown here is smaller than that of the model climatology (i.e., $r = -0.83$) and results of previous studies [*Neelin et al*., 2013; *Chang et al*., 2015], it is still statistically significant at the 95% confidence level.

To better understand the uncertainty of the E-NPSH latitude trends, the SLP and precipitation changes are separately examined for the models with E-NPSH-N and E-NPSH-S in Figure 5. The two groups of models show substantial differences (see Figure 5c). For example, the E-NPSH-N models (Figure 5a) exhibit increase of SLP on the poleward side of the climatological NPSH, consistent with a poleward displacement of the E-NPSH latitude. In these models, precipitation changes over California are generally weak and insignificant. The trend of the area-averaged precipitation over the red box in the figure is only 0.014 mm/d/decade (see the red dot in Figure 4b). In contrast, the E-NPSH-S models (Figure 5b) show eastward and southward expansion of the AL in the 21st century, indicating an equatorward shift of storm tracks. Accordingly, California winter precipitation is simulated to increase substantially (0.086 mm/d/decade; see the blue dot

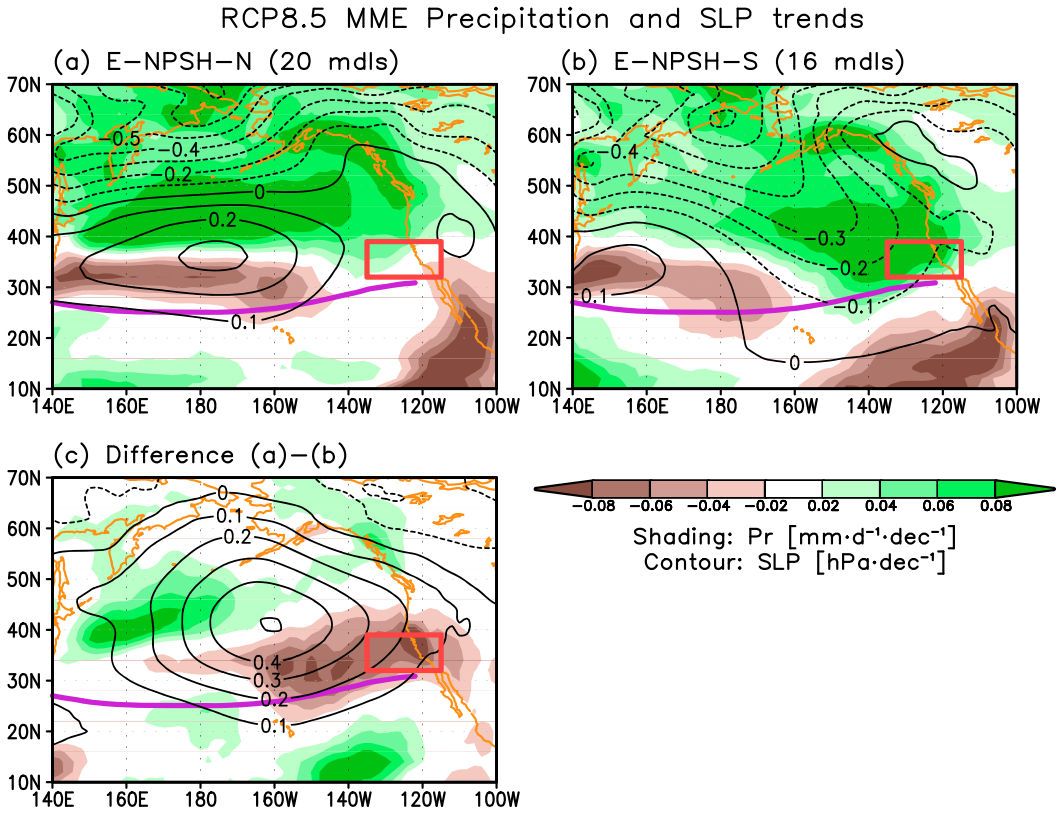

Figure 5. Projected future changes of DJF sea level pressure (contours) and precipitation (shading) for the models of (a) the northward shift (E-NPSH-N) and (b) the southward shift of the E-NPSH (E-NPSH-S). (c) Difference between Figures 5a and 5b.

in Figure 4b). Thus, a considerable intermodel spread in the projected California precipitation changes can be attributed to the uncertainty in the projected changes in the E-NPSH latitude.

3.3. Constraints on NPSH Changes

What causes the intermodel spread in the projected changes in W-NPSH and E-NPSH latitudes? To better understand the uncertainty in the projected atmospheric circulation changes, this section addresses the factors that potentially control the NPSH change and its zonal asymmetry under global warming. Since the latitudinal location of the subtropical high is dynamically linked to the HC boundary, we adopt the approach that has been often taken to study the HC expansion [e.g., *Lu et al*., 2008]. From a zonal mean perspective, the poleward boundary of the HC, adjoining the subtropical ridge, tends to reach the latitude where baroclinic instability occurs [*Held*, 2000]. *Lu et al*. [2008] evaluated the changes in baroclinicity under global warming and its impacts on the HC boundary by using the baroclinic criticality [*Phillips*, 1954]:

$$C = \frac{f^2(u_{500} - u_{850})}{\beta g H(\theta_{500} - \theta_{850})/\Theta_0}, \tag{1}$$

where the zonal wind (u) shear and potential temperature (θ) gradient are taken between 500 hPa and 850 hPa. H represents the air column thickness between 500 hPa and 850 hPa and is set to be a constant. Other symbols are standard. *Lu et al*. [2007, 2008] documented that the increased static stability of the subtropical troposphere under global warming may stabilize the westerly jet and delay its baroclinic instability till higher latitude, as such giving rise to a poleward expansion of the HC. In contrast, the increased vertical wind shear could enhance the eddy activity in the subtropics and result in a contraction of the HC.

The above scaling analysis has typically been applied to the zonal mean circulation. In this study, the scaling analysis is applied to regional circulation changes in order to qualitatively evaluate the relative importance of zonal wind shear (u_{500}–u_{850}) and static stability (θ_{500}–θ_{850}) changes in the NPSH latitude changes. Following

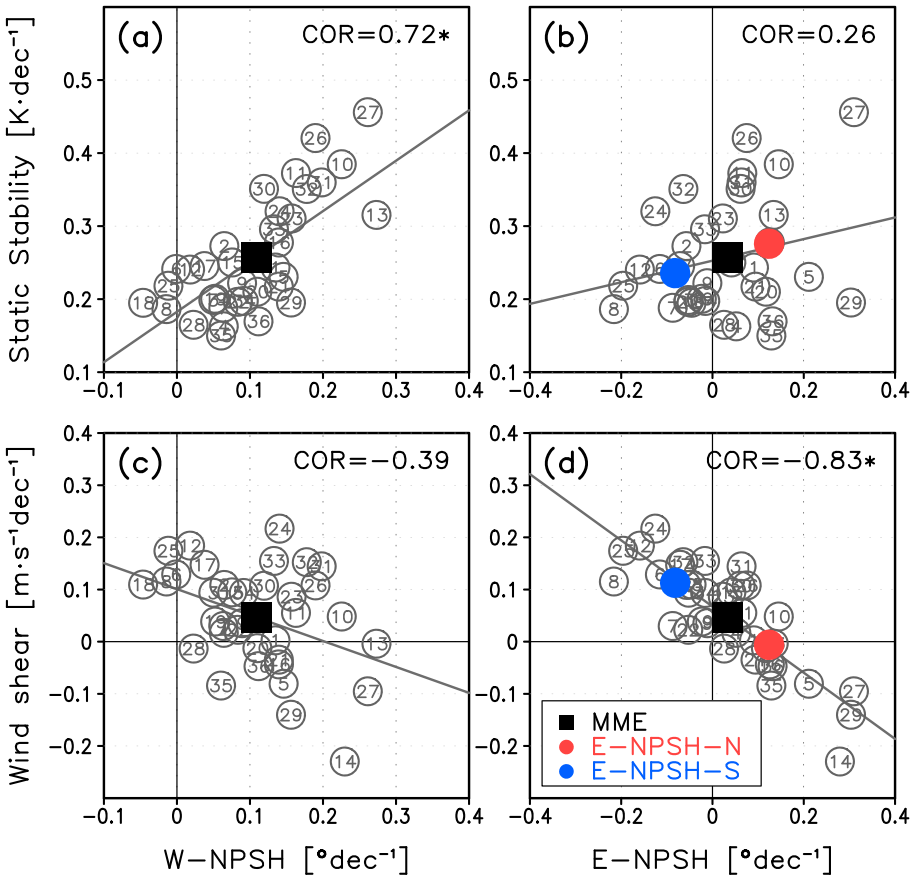

Figure 6. (a) Relationship between the projected changes of the W-NPSH latitude and static stability. (b) Same as Figure 6a but for the E-NPSH latitude. (c and d) Same as Figures 6a and 6b but for the vertical wind shear on the *Y* axis. The static stability and vertical wind shear are averaged over 20°–40°N and 140°E–120°W. Red and blue circles in Figures 6b and 6d indicate the MME of the selected models showing positive and negative trends of E-NPSH latitudes, respectively.

Lu et al. [2008], these two factors are computed around the equatorward side of the westerly jet (20°–40°N) over the Pacific basin (140°E–120°W).

Figure 6 exhibits the relationship between the factors of baroclinic criticality trends and NPSH latitude trends. The projected changes in the W-NPSH latitudes are strongly correlated with the increase in the subtropical static stability (θ_{500}–θ_{850}) with a correlation coefficient of 0.72 (Figure 6a). Only a weak relationship is found with the vertical wind shear (u_{500}–u_{850}) changes (Figure 6c). This result indicates that the intermodel spread of the W-NPSH latitude trends is associated with the uncertainty in the projected changes in the subtropical static stability over the North Pacific. However, this is not the case for the E-NPSH latitude trends. The intermodel spread of the projected change of the E-NPSH latitude is strongly related with that of the vertical wind shear. The correlation coefficient between the two is −0.83 (Figure 6d). In contrast, only a weak relationship is found with static stability change ($r = 0.26$; Figure 6b). More importantly, while the static stability changes are positive in all models, the vertical wind shear changes show both positive and negative trends (i.e., E-NPSH-N is −0.01 m/s/decade and E-NPSH-S is 0.11 m/s/decade). This result suggests that while the uncertainty of the W-NPSH latitude trends is primarily associated with thermodynamic changes, that of the E-NPSH latitude trends is related with dynamical circulation changes.

A great caution should be exercised in interpreting the scaling analysis above, which should be applicable to the thermally forced wind. While the upstream portion of the Asia-Pacific jet is predominantly thermally forced, the wind downstream over the eastern Pacific is more eddy driven. Therefore, the high correlation between the E-NPSH latitude and the vertical wind shear in Figure 6d may just reflect nothing more than the thermal wind relation. Nevertheless, further evidence will be provided below showing that indeed, the

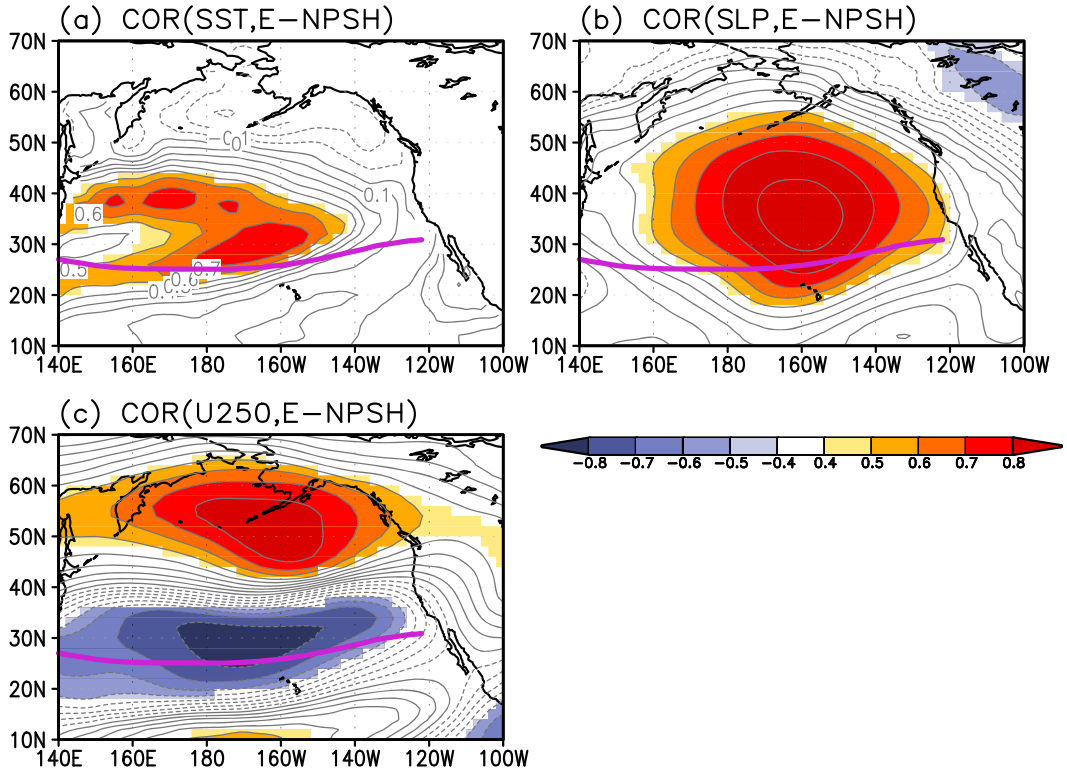

Figure 7. (a) Correlation between the sea surface temperature (SST) trends and E-NPSH latitude trends. (b and c) Same as Figure 7a but for sea level pressure (SLP) and zonal wind at 250 hPa (U250), respectively.

enhanced wind shear can be accounted for by the increased thermal gradient from the change of sea surface temperature (SST).

Figure 7a shows the correlation map of the SST trends with the intermodel spreads of E-NPSH latitudes trends. Similar maps are also presented for SLP and 250 hPa zonal wind in Figures 7b and 7c. Consistent with *Langenbrunner et al*. [2015, Figure 7a], Figure 7a indicates that the intermodel spread in the projected change in the E-NPSH latitude is strongly associated with uncertainty in the SST change over the western North Pacific instead of the eastern North Pacific. Such SST pattern resembles a Pacific Decadal Oscillation (PDO)-like sea surface temperature signature in the midlatitudes. This PDO-like SST change tends to increase (decrease) magnitude of latitudinal temperature gradient north (south) of 30°–40°N, leading to a poleward shift in the westerly jet, as shown in Figure 7c. They are also related to an enhanced anticyclonic circulation over the North Pacific centered at 160°W and 40°N (SLP in Figure 7b), a pattern that is almost identical to the SLP difference between the models with E-NPSH-N and E-NPSH-S (see Figure 5c). This result suggests that midlatitude air-sea coupling can serve as a major source of uncertainty for the projected changes of E-NPSH latitudes and California winter precipitation.

To elucidate the leading patterns of model-to-model spread in atmospheric circulation linked to surface temperature trends, a SVD analysis on winter SLP and SST trends following *Bretherton et al*. [1992] is also performed (Figure 8). Here the leading SVD mode, shown in Figures 8a and 8b, denotes the model-to-model spread around the MME. For instance, the models with a negative sign of PC of SST, their future projection shows the SST warming (not PDO-like cooling) but with a relatively weak magnitude compared to the MME mean. The leading mode, which explains 62.3% of the total squared covariance, resembles a PDO-like pattern as shown in Figure 7a [see also *Langenbrunner et al*., 2015, Figure 7a]. The magnitude of warming reaches 0.12 K/decade near the Kuroshio-Oyashio extension region. Although the center of the surface circulation change differs slightly from that in Figure 7b, an enhanced anticyclonic circulation, corresponding to the PDO-like midlatitude warming, is also evident (Figure 8b). This result points to the intermodel difference in the surface temperature trends in the *western* North Pacific, and the related feedback processes

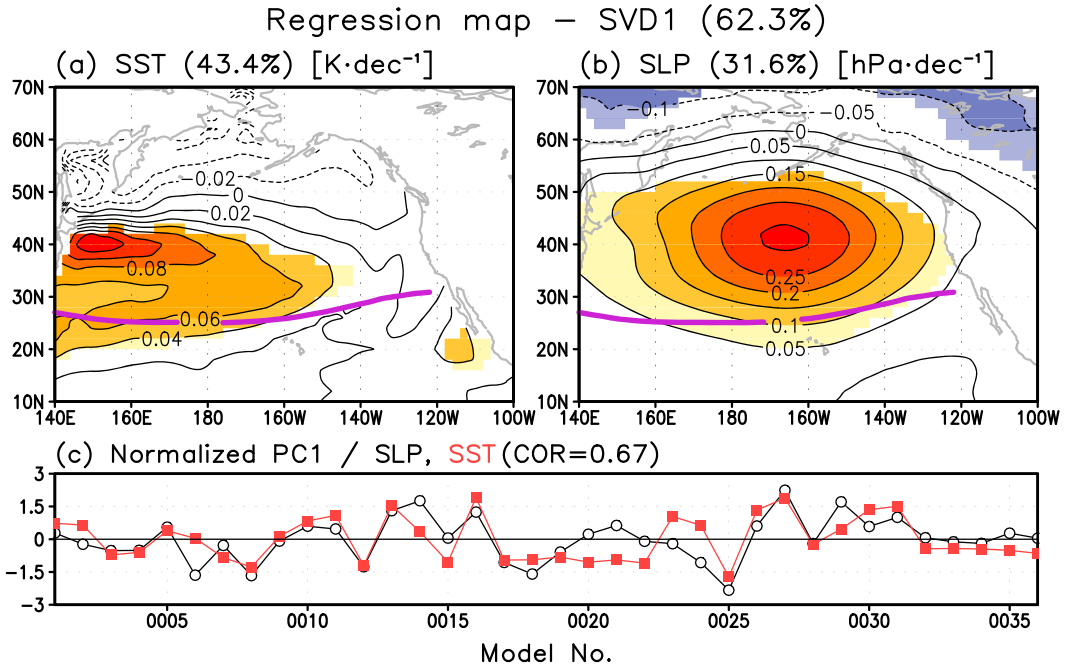

Figure 8. Regression map against the leading principal component of the singular value decomposition (SVD) mode for (a) sea surface temperature and (b) sea level pressure. (c) Normalized principal components of the leading SVD mode. The *X* axis in Figure 8c indicates the model number as listed in Table 1.

are as the major factors for the intermodel uncertainty in the projections of the E-NPSH latitude and California winter precipitation.

One might wonder whether the spread in the projected shift in E-NPSH can be related to the mean bias of the circulation index, as has been found for the Southern Hemisphere in previous studies [*Kidston and Gerber*, 2010; *Son et al.*, 2010]. To this end, we examine in Figure 9 the relationship between the projected shift of E-NPSH latitudes and the model bias (i.e., model climatology minus HadSLP2 observation) in the latitudes of E-NPSH and W-NPSH. It is found that an equatorward bias in W-NPSH latitudes is linked to a greater poleward shift of E-NPSH with a correlation coefficient of −0.49 (Figure 9a). Somewhat surprisingly, this correlation is higher than that against the bias in E-NPSH latitude (Figure 9b; $r = -0.38$). This result again suggests that faithful representation of the air-sea coupling over the western North Pacific, which results in

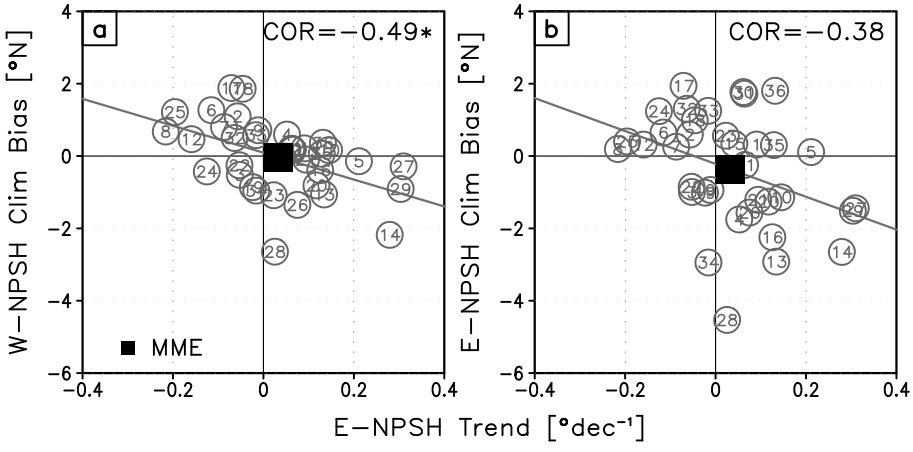

Figure 9. Scatterplot of the projected future changes of the E-NPSH latitudes and climatological locations of (a) W-NPSH and (b) E-NPSH latitudes. Each number denotes the model number as listed in Table 1. The filled square indicates the MME.

the correct position of the W-NPSH, might help reduce the uncertainty in the projection of California winter precipitation. Moreover, if the model mean bias has any guiding value, models with equatorward (poleward) biased W-NPSH latitudes may project less (more) winter precipitation for California than the reality.

4. Summary and Discussion

This study assesses large-scale atmospheric circulation change over the North Pacific in a future climate and the associated uncertainty, with implications for winter precipitation change in California. Since California is located at the transitional region between the Pacific storm track and a subtropical dry zone, its precipitation changes are likely controlled by multiple processes [e.g., *Langenbrunner et al.*, 2015]. Accordingly, model biases and uncertainty in thermodynamical and dynamical processes can easily lead to considerable uncertainty in the projected changes in Californian winter precipitation. Two indices, W-NPSH and E-NPSH latitudes, are defined as proxies for the location of the local HC edge to quantify the North Pacific atmospheric circulation and its response to global warming. The location of the E-NPSH is highly correlated with California winter precipitation in both the model mean bias and future projections under the RCP8.5 scenario.

The CMIP5 models show strong agreement on the poleward displacement of the W-NPSH latitudes under the RCP8.5 scenario. Most models predict a decrease in high-latitude SLP but an increase in midlatitude SLP over the W-NPSH region. This poleward shift of the W-NPSH latitude, or local expansion of the HC, may be explained by an increase of static stability in the subtropical North Pacific. As such, the similar mechanism for the poleward expansion of the zonal mean Hadley cell may be also operating for the local poleward shift of the NPSH in the western Pacific.

The E-NPSH latitudes do not show systematic trends under the RCP8.5 scenario. The models are equivocal about which way the E-NPSH will shift in a warmer climate. The MME projects almost no change in E-NPSH latitude with a larger model-to-model spread than W-NPSH. For example, the magnitude of the projected California precipitation changes under the RCP8.5 scenario can differ by a factor of 6 depending on the sign and the magnitude of the E-NPSH latitude trends. This uncertainty, which is closely linked to the uncertain change in California winter precipitation, is related to the uncertainty in the changes of the vertical wind shear at the equatorward side of the Pacific jet. This uncertainty can be further linked to a PDO-like SST pattern and the associated baroclinicity. Taken together, this suggests that a certain amount of intermodel spread in the projected changes of the E-NPSH latitude and California winter precipitation is rooted in the midlatitude atmosphere-ocean coupled dynamics over the western North Pacific.

Our result is consistent with the recent studies relating California winter precipitation change in a warmer climate to large-scale features such as the storm track and Pacific jet extent [*Chang et al.*, 2015; *Langenbrunner et al.*, 2015]. A consensus emerging from these studies is that the uncertainty in the future wintertime California precipitation is much greater than the intermodel agreement, a factor that must be taken into consideration in the planning for adaptation and mitigation to the projected hydroclimate changes in California.

Acknowledgments

This work was funded by the Korea Meteorological Administration Research and Development Program under grant KMIPA 2015-2100. J.L. and J.Y. were supported by the Office of Science of the U.S. Department of Energy as part of the Regional and Global Climate Modeling program. D.M.W.F. is supported by NSF grants AGS-0846641, AGS-0936059, AGS-1359464, and PLR-1341497 and a UW Royalty Research Fund grant. We acknowledge the World Climate Research Programme's Working Group on Coupled Modelling, which is responsible for CMIP, and we thank the climate modeling groups (listed in Table 1 of this paper) for producing and making available their model output. For CMIP, the U.S. Department of Energy's Program for Climate Model Diagnosis and Intercomparison provides coordinating support and led the development of software infrastructure in partnership with the Global Organization for Earth System Science Portals. The HadSLP2 data were obtained from the Met Office Hadley Centre (http://www.metoffice.gov.uk/hadobs/hadslp2/). The GPCP data were provided by the NASA (http://precip.gsfc.nasa.gov/gpcp_v2.2_data.html). The CMAP data were available from the NOAA CPC ftp server (ftp://ftp.cpc.ncep.noaa.gov/precip/cmap). The JRA-55 data were provided by JMA (ftpds.data.jma.go.jp).

References

Adler, R. F., et al. (2003), The version 2 Global Precipitation Climatology Project (GPCP) Monthly Precipitation Analysis (1979–present), *J. Hydrometeorol.*, *4*, 1147–1167.

Allan, R., and T. Ansell (2006), A new globally complete monthly historical gridded mean sea level pressure dataset (HadSLP2): 1850–2004, *J. Clim.*, *19*, 5816–5842.

Barnes, E. A., and L. Polvani (2013), Response of the midlatitude jets, and of their variability, to increased greenhouse gases in the CMIP5 models, *J. Clim.*, *26*, 7117–7135.

Bretherton, C. S., C. Smith, and J. M. Wallace (1992), An intercomparison of methods for finding coupled patterns in climate data, *J. Clim.*, *5*, 541–560.

Chang, E. K. M. (2013), CMIP5 projection of significant reduction in extratropical cyclone activity over North America, *J. Clim.*, *26*, 9903–9922.

Chang, E. K. M., S. Lee, and K. L. Swanson (2002), Storm track dynamics, *J. Clim.*, *15*, 2163–2183.

Chang, E. K. M., Y. Guo, and X. Xia (2012), CMIP5 multimodel ensemble projection of storm track change under global warming, *J. Geophys. Res.*, *117*, D23118, doi:10.1029/2012JD018578.

Chang, E. K. M., C. Zheng, P. Lanigan, A. M. W. Yau, and J. D. Neelin (2015), Significant modulation of variability and projected change in California winter precipitation by extratropical cyclone activity, *Geophys. Res. Lett.*, *42*, 5983–5991, doi:10.1002/2015GL064424.

Choi, J., S.-W. Son, J. Lu, and S.-K. Min (2014), Further observational evidence of Hadley cell widening in the Southern Hemisphere, *Geophys. Res. Lett.*, *41*, 2590–2597, doi:10.1002/2014GL059426.

Frierson, D. M. W. (2006), Robust increases in midlatitude static stability in simulations of global warming, *Geophys. Res. Lett.*, *33*, L24816, doi:10.1029/2006GL027504.

Frierson, D. M. W., J. Lu, and G. Chen (2007), The width of the Hadley circulation in simple and comprehensive general circulation models, *Geophys. Res. Lett.*, *34*, L18804, doi:10.1029/2007GL031115.

Gao, Y., L. R. Leung, J. Lu, Y. Liu, M. Huang, and Y. Qian (2014), Robust spring drying in the southwestern U.S. and seasonal migration of wet/dry patterns in a warmer climate, *Geophys. Res. Lett.*, *41*, 1745–1751, doi:10.1002/2014GL059562.

Gerber, E. P., and S.-W. Son (2014), Quantifying the summertime response of the austral jet stream and Hadley cell to stratospheric ozone and greenhouse gases, *J. Clim.*, *27*, 5538–5559.

Held, I., and B. Soden (2006), Robust responses of the hydrological cycle to global warming, *J. Clim.*, *19*, 5686–5699.

Held, I. M. (2000), *The General Circulation of the Atmosphere, Paper Presented at 2000 Woods Hole Oceanographic Institute Geophysical Fluid Dynamics Program*, Woods Hole Oceanogr. Inst, Woods Hole, Mass.

Hu, Y., C. Zhou, and J. Liu (2011), Observational evidence for the poleward expansion of the Hadley circulation, *Adv. Atmos. Sci.*, *28*, 33–44.

Hwang, Y.-T., D. M. W. Frierson, and S. M. Kang (2013), Anthropogenic sulfate aerosol and the southward shift of tropical precipitation in the 20th century, *Geophys. Res. Lett.*, *40*, 1–6, doi:10.1002/grl50502.

Intergovernmental Panel on Climate Change (IPCC) (2013), Climate change 2013: The physical science basis, in *Contribution of Working Group I to the Fifth Assessment Report of the Intergovernmental Panel on Climate Change*, edited by T. F. Stocker et al., 1535 pp., Cambridge Univ. Press, Cambridge, U. K., and New York, doi:10.1017/CBO9781107415324.

Kalnay, E., et al. (1997), The NCEP/NCAR 40-year reanalysis project, *Bull. Am. Meteorol. Soc.*, *77*, 437–471.

Kidston, J., and E. P. Gerber (2010), Intermodel variability of the poleward shift of the austral jet stream in the CMIP3 integrations linked to biases in 20th century climatology, *Geophys. Res. Lett.*, *37*, L09708, doi:10.1029/2010GL042873.

Kobayashi, S., et al. (2015), The JRA-55 reanalysis: General specifications and basic characteristics, *J. Meteorol. Soc. Jpn.*, *93*(1), 5–48, doi:10.2151/jmsj.2015-001.

Kwon, Y.-O., M. A. Alexander, N. A. Bond, C. Frankignoul, H. Nakamura, B. Qiu, and L. A. Thompson (2010), Role of the Gulf Stream and Kuroshio–Oyashio systems in large-scale atmosphere-ocean interaction: A review, *J. Clim.*, *23*, 3249–3281.

Langenbrunner, B., J. D. Neelin, B. R. Lintner, and B. T. Anderson (2015), Patterns of precipitation change and climatological uncertainty among CMIP5 models, with a focus on the midlatitude Pacific storm track, *J. Clim.*, *28*, 7857–7872.

Lu, J., G. A. Vecchi, and T. Reichler (2007), Expansion of the Hadley cell under global warming, *Geophys. Res. Lett.*, *34*, L06805, doi:10.1029/2006GL028443.

Lu, J., G. Chen, and D. M. W. Frierson (2008), Response of the zonal mean atmospheric circulation to El Niño versus global warming, *J. Clim.*, *21*, 5835–5851.

Manabe, S., and R. T. Wetherald (1975), The effects of doubling the CO_2 concentration on the climate of a general circulation model, *J. Atmos. Sci.*, *32*, 3–15.

Neelin, J. D., B. Langenbrunner, J. E. Meyerson, A. Hall, and N. Berg (2013), California winter precipitation change under global warming in the Coupled Model Intercomparison Project Phase 5 ensemble, *J. Clim.*, *26*, 6238–6256.

Park, J.-H., and S.-I. An (2014), Southward displacement of the upper atmosphere zonal jet in the eastern north Pacific due to global warming, *Geophys. Res. Lett.*, *41*, 7861–7867, doi:10.1002/2014GL062175.

Phillips, N. A. (1954), Energy transformations and meridional circulations associated with simple baroclinic waves in a two-level, quasi-geostrophic model, *Tellus*, *6*, 273–286.

Scheff, J., and D. M. W. Frierson (2012a), Twenty-first-century multimodel subtropical precipitation declines are mostly midlatitude shifts, *J. Clim.*, *25*, 4330–4347.

Scheff, J., and D. M. W. Frierson (2012b), Robust future precipitation declines in CMIL5 largely reflect the poleward expansion of model subtropical dry zones, *Geophys. Res. Lett.*, *39*, L18704, doi:10.1029/2012GL052910.

Seo, K.-H., D. M. W. Frierson, and J.-H. Son (2014), A mechanism for future changes in Hadley circulation strength in CMIP5 climate change simulations, *Geophys. Res. Lett.*, *40*, 5251–5258, doi:10.1002/2014GL060868.

Son, S.-W., et al. (2010), Impact of stratospheric ozone on Southern Hemisphere circulation change: A multimodel assessment, *J. Geophys. Res.*, *115*, D00M07, doi:10.1029/2010JD014271.

Trenberth, K. E. (2011), Changes in precipitation with climate change, *Climate Res.*, *47*, 123–138, doi:10.3354/cr00953.

Xie, P., and P. A. Arkin (1997), Global precipitation: A 17-year monthly analysis based on gauge observations, satellite estimates, and numerical model outputs, *Bull. Am. Meteorol. Soc.*, *78*, 2539–2558.